Journal of Materials Chemistry C

ROYAL SOCIETY OF CHEMISTRY

PAPER

View Article Online
View Journal | View Issue

Cite this: J. Mater. Chem. C, 2023, 11, 656

Ultra-fast low temperature scintillation and X-ray luminescence of $CsPbCl_3$ crystals

V. B. Mykhaylyk, *[a] M. Rudko,[b] H. Kraus,[c] V. Kapustianyk,[b] V. Kolomiets,[b] N. Vitoratou,[a] Y. Chornodolskyy,[d] A. S. Voloshinovskii[d] and L. Vasylechko[e]

Halide perovskites recently emerged as promising materials for the detection of ionising radiation. Single crystals of halide perovskites exhibit very fast and bright scintillation when cooled and may outperform the best modern scintillators at temperatures below 100 K. In this work we report on low-temperature scintillation properties of $CsPbCl_3$ single crystals, grown using the Bridgeman method. The temperature dependences of the luminescence and decay kinetics were studied using X-ray excitation. At low temperatures, the crystal exhibits an intense narrow-band emission at about 420 nm with very fast decay kinetics. This emission, of which a characteristic feature is the strong thermal quenching, is attributed to the radiative decays of bound and trapped excitons. The fast, middle, and slow decay time constants obtained from a fit of a sum of exponential functions to the decay curve at 10 K are 0.1, 1 and 11 ns, respectively. The scintillation light yield of $CsPbCl_3$ at 7 K measured at excitation with α-particles from an ^{241}Am source is estimated to be 140 ± 15% of a reference LYSO-Ce crystal and 19000 ± 2000 ph per MeV under 14 keV X-ray excitation at 10 K. It is concluded that owing to a reduced amplitude of the slow decay component, $CsPbCl_3$ exhibits an ultra-fast scintillation response that is superior to that of other halide perovskites. The combination of sub-nanosecond response time and the encouraging light yield has the potential of establishing this material as first choice for scintillation applications that rely on prompt detector response at cryogenic temperatures.

Received 31st October 2022,
Accepted 16th November 2022

DOI: 10.1039/d2tc04631h

rsc.li/materials-c

1. Introduction

Scintillation materials with high efficiency and fast response are increasingly important for the detection of ionising radiation. Successful applications of halide perovskites to direct detection of X-rays,[1,2] raised expectations regarding a future role of halide perovskites in high-energy radiation detection,[3] and prompted further studies of their scintillation properties. Lead halide perovskite nanocrystals emerged recently as a potential new generation of scintillating materials that exhibit a high light yield and a very fast decay time.[4–8] Subsequently, recent years witnessed a surge in research activity in this area and many pertinent publications were promptly summarised in a couple of reviews.[9–11] Halide perovskite nanocrystals used for scintillation detection exhibit excellent performance, but there are also a number of limitations. The exceptional emission characteristics of these nanocrystals, in particular the impressive brightness at room temperature, are due to the favourable combination of two fundamental factors. The first is a quantum confinement effect that prevents thermal quenching and results in a quantum yield of exciton luminescence close to 100%.[12] Second, because of the small dimensions of nanocrystals the near-edge exciton emission has high probability for escaping the volume of the nanocrystal without absorption. It is due to this second factor, that the excellent scintillation properties of these nanoparticles are best put to use when they are prepared as thin (~100 μm) films,[4,5,13,14] dispersed in a plastic matrix,[6,15,16] or other crystal hosts.[7,17] However, when it comes to the absorption of ionising radiation this method has a problem. Spectroscopic detection of hard X-rays relies on photoelectric absorption which is a function of absorber composition and thickness. In case of bulk halide perovskites, in order to fully absorb 100 keV X-rays, a material thickness of at least 1 mm is required.[2] This is currently not achievable when using film or dispersed nanocrystals.[18] Therefore, the usefulness of single-crystal scintillators for the detection of high-energy radiation is well-worth investigating.

The concept of applying halide perovskites as scintillation detector of ionising radiation has been discussed since the first observation of the very fast and intense exciton luminescence of

[a] Diamond Light Source, Harwell Campus, Didcot, OX11 0DE, UK. E-mail: vmikhai@hotmail.com
[b] Scientific-technical and Educational Centre of low Temperature Studies, I. Franko National University of Lviv, 50 Dragomanova str., 79005, Lviv, Ukraine
[c] University of Oxford, Department of Physics, Denys Wilkinson Building, Keble Road, Oxford, OX1 3RH, UK
[d] I. Franko National University of Lviv, Physics Department, 8 Kyrylo and Mefodiy str., 79005, Lviv, Ukraine
[e] Lviv Polytechnic National University, S. Bandera str. 12, Lviv 79013, Ukraine

$CsPbX_3$ (X = Cl, Br, I) at low temperatures.[19] However, the emission intensity is very temperature dependant due to thermal quenching.[20] The scintillation light yield of $CsPbX_3$ single crystals is less than 1000 ph per MeV at room temperatures,[21,22] but drastically increases with cooling below 100 K.[23] This temperature range is important for specialised particle physics experiment where the use of cryogenic detectors for ionising radiation facilitates an appreciable enhancement of sensitivity.[24,25] Furthermore, the feasibility of employing fast cryogenic scintillators in nuclear imaging[26] and non-contact thermometry[27] is actively investigated. Thus, taking into account the excellent light yield and very fast decay time observed in halide perovskites at low temperature,[8,23,28] we envisage opportunities for this family of materials in scintillator-based applications at cryogenic temperatures. This motivated us to investigate the X-ray luminescence and scintillation characteristics of $CsPbCl_3$ from room temperature down to 7 K. The purpose of the study is, by exploring and analysing the temperature dependence of these properties, to assess the potential of the material as cryogenic scintillation detector. Our findings complement recent results for other lead halide perovskites.[8,23,28]

2. Methods

The sample of a $CsPbCl_3$ crystal used in this study was grown by the Bridgeman technique from a stoichiometric mixture of high-purity CsCl and $PbCl_2$ sealed in a quartz ampoule. Because $CaPbCl_3$ crystal is only mildly hygroscopic it was cut and polished at ambient conditions. The samples prepared in such way where then kept in sealed jar with silica gel granules and exhibited no visible degradation after storage over more than a year.

Phase and structural characterization of $CsPbCl_3$ was performed by X-ray powder diffraction (XRD) technique using Aeris benchtop diffractometer (Malvern Panalytical) equipped with PIXcel^{1D} strip detector. Experimental diffraction data were collected using filtered Cu K_α radiation (λ = 1.54185 Å) in a 2θ range of 10–105 degrees with a 2θ step of 0.01°. Crystal structure parameters (unit cell dimensions, coordinates and displacement parameters of atoms) were derived from experimental XRD pattern by full profile Rietveld refinement using WinCSD software package.[29]

The luminescence studies were performed on a freshly polished crystal sample of a volume of 5 × 5 × 4 mm^3. For X-ray luminescence measurements the sample was placed into a closed-cycle He cryostat, equipped with a DE-202A cryocooler (Advanced Research Systems) and Cryocon 32 (Cryogenic Control Systems Inc.) temperature regulator. The luminescence was excited by a URS-55A X-ray tube with a Cu-anticathode operating at 55 kV and 10 mA. The X-ray beam was entering the cryostat through a beryllium window and irradiated the sample holder placed at 45° to the incoming radiation. The emission was collected in reflection mode through a quartz window of the cryostat. The luminescence spectra were measured using a monochromator MDR-12 and photomultiplier module Hamamatsu H9305.

The decay curves of the crystals were measured at the B16 beamline of Diamond Light Source synchrotron using a 14 keV monochromatic X-ray beam. The measurements were carried out in hybrid mode by triggering on a single X-ray pulse with FWHM of Δt = 60 ps, separated from the following pulses by a 300 ns gap. The single crystal, attached to a holder, was placed in a continuous-flow, He-cryostat (Oxford Instruments). The sample temperature was monitored using a Si-diode sensor and stabilised by a PID controller. The X-ray beam with a flux of approx. 10^9 ph per (s·mm^2) was impinging upon the sample placed at 45° to the incoming radiation through a 0.2 mm thick aluminised Mylar window. The luminescence from the illuminated area of 2 × 2 mm^2 was collected in reflection mode at 45° through a quartz window. Taking into account the penetration depth of 14 keV X-ray (*ca.* 20 μm) and absorption coefficient of $CsPbCl_3$ at the emission peak 420 nm at 10 K (*ca.* 30 cm^{-1})[30] we estimate that in this geometry more than 95% of scintillation light can escape the crystal. The emission was detected using an ID100 single photon counting detector with timing resolution 40 ps sensitive over a 400–900 nm spectral range and a PICO Harp 300 time-correlated single photon counting module.

To measure scintillation properties as function of temperature we used the multiphoton counting technique described in.[31] The sample was attached to the copper sample holder with the ^{241}Am source placed behind the sample inside a He-flow cryostat. The signal was detected by a multi-alkali photomultiplier model 9124A (Electron Tubes Enterprises). The measurements were carried out while cooling the crystal to eliminate a spurious signal from thermoluminescence.

Density of states (DOS) calculations were carried out using the Quantum-Espresso package.[32] The exchange–correlation functional was chosen in the Perdew–Burke–Ernzerhof generalized gradient approximation, modified for solids with Hubbard correction (GGA-PBEsol+U). The U parameter was selected at 5 eV and applied to Cl p-states. The 3 × 3 × 3 Monkhorst-Pack mesh was used for the k-point sampling of the Brillouin zone of $CsPbCl_3$.

3. Results and discussion

3.1. Crystal structure

Examination of XRD pattern of powdered $CsPbCl_3$ crystal revealed pure orthorhombic perovskite structure in accordance with ICDD PDF-4 card N 04-024-6243. No traces of impurity phases were detected. Phase purity and crystal structure of the investigated material was further confirmed by full profile Rietveld refinement, performed in space groups *Pnma*. The atomic positions in $CsPbCl_3$ structure derived from high-resolution X-ray synchrotron powder diffraction[33] were used as a starting model for the refinement. In the refinement procedure, the unit cell dimensions, positions and displacement parameters of atoms and site occupancies were refined together with profile parameters and corrections for instrumental sample shift. As the result, an excellent agreement between experimental and calculated XRD profiles was achieved (see Fig. 1). All the

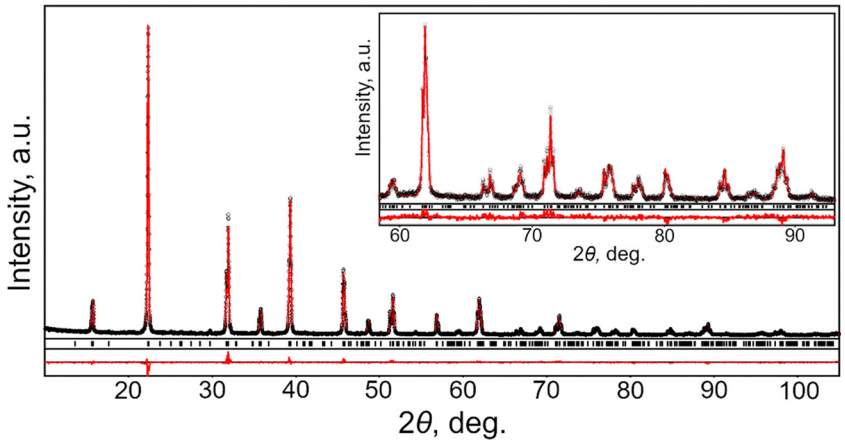

Fig. 1 Graphical results of Rietveld refinement of $CsPbCl_3$ structures. Experimental XRD pattern (small red circles) is shown in comparison with calculated pattern (black line). Short vertical bars indicate the positions of Bragg's maxima in the orthorhombic perovskite structure. Inset shows enlarged high-angles part of the pattern.

features of experimental powder diffraction pattern of $CsPbCl_3$ were successfully modelled in space group *Pnma* with the $\sqrt{2}a_p \times 2a_p \times \sqrt{2}a_p$ metrics of orthorhombic cell. No indications of monoclinic distortion of the structure were observed at room temperature. Obtained structural parameters of $CsPbCl_3$ and the final residuals are presented in Table 1. Selected interatomic distances and angles in $CsPbCl_3$ structure derived from the refined values of the lattice parameters and atomic coordinates are collated in Table 2.

The results obtained in the present study prove orthorhombic $GdFeO_3$-type of perovskite structure of $CsPbCl_3$, being in agreements with abovementioned comprehensive examination of this material,[33] as well as with the recent temperature-dependent high resolution synchrotron powder diffraction investigations in the temperature range 90–823 K.[34] According to the latter study, $CsPbCl_3$ undergoes two successive phase transitions from ideal cubic $Pm\bar{3}m$ perovskite to tetragonal $P4/mbm$ structure at 325 K and finally to orthorhombic *Pbnm* (*Pnma*) structure at 316 K.

Room temperature structure of $CsPbCl_3$ belongs to the most widespread family of ABO_3 perovskite structures, namely $GdFeO_3$-type, which is characterised by anti-phase tilting of the corner-shared BO_6 octahedra according to Glazer tilt system $a^-b^+a^-$. Magnitudes of octahedra tilt angles about the cubic [001] and [110] axes can be estimated from the deviation of Pb–Cl1–Pb and Pb–Cl2–Pb bond angles (Table 2) from 180°, respectively. The $PbCl_6$ octahedra in $CsPbCl_3$ structure are slightly distorted due to the deviation of the Pb–Cl distances from the average value of 2.836 Å (Table 2) and Cl–Pb–Cl bond angles (not shown here) inside octahedra from 90°. The distorted cubooctahedral holes in $CsPbCl_3$ structure are occupied by cesium ions. Distribution of Cs–Cl distances inside $CsCl_{12}$ polyhedra is non-uniform: two shortest Cl atoms are located at the distance of 3.488 Å from the central Cs atom, whereas two remote Cl species lie at the distance of 4.474 Å (Table 2).

Table 2 Selected interatomic distances in $CsPbCl_3$ structure

Atoms	Distances, Å	Atoms	Distances, Å	Atoms	Angles, deg.
Cs–Cl1 × 2	3.488(10)	Pb–Cl1 × 2	2.787(13)	Pb–Cl1–Pb	160.08(4)
Cs–Cl2	3.580(10)	Pb–Cl2 × 2	2.839(2)	Pb–Cl2–Pb	164.06(4)
Cs–Cl2	3.806(14)	Pb–Cl1 × 2	2.883(12)		
Cs–Cl2 × 2	3.885(10)	Pb–Cl(ave)	2.836		
Cs–Cl2 × 2	4.062(11)				
Cs–Cl1	4.126(14)				
Cs–Cl1	4.333(10)				
Cs–Cl2 × 2	4.474(11)				

3.2. X-ray luminescence

Emission properties of $CsPbCl_3$ are known to be very sensitive to the temperature, and that is clearly manifested in X-ray luminescence spectra of the crystal (see Fig. 2). X-ray excitation of the crystals at 10 K reveals a structured luminescence spectrum with two narrow peaks at 417 nm (1) and 421 nm (2) with a broad shoulder (3) on the low-energy side of the

Table 1 Lattice parameters, coordinates and displacement parameters of atoms in $CsPbCl_3$ structure at room temperature (space group *Pnma*, $Z = 4$)

Lattice parameters, residuals	Atoms, sites	x/a	y/b	z/c	$B_{iso/eq}$, Å^2	Occupancy
a = 7.8994(3) Å	Cs, 4*c*	0.5042(5)	$\frac{1}{4}$	0.0039(9)	4.16(4)	0.995(5) Cs^+
b = 11.2459(2) Å	Pb, 4*a*	0	0	0	0.40(2)	1.002(5) Pb^{+4}
c = 7.8960(3) Å	Cl1, 4*c*	−0.0435(13)	$\frac{1}{4}$	−0.024(2)	1.9(2)	1.01(1) Cl^-
	Cl2, 8*d*	0.209(2)	−0.0232(5)	0.717(2)	1.54(14)	1.03(2) Cl^-

R_I = 0.038, R_P = 0.090

spectra. The measured X-ray luminescence spectrum exhibits a pronounced change with temperature. The overall emission intensity decreases with heating due to non-radiative quenching processes. The narrow peak 1 is manifest only at low temperatures and its position in energy at 2.97 eV is very close to the low-temperature exciton absorption of $CsPbCl_3$. The position of this peak agrees with the published data on photoluminescence of bulk crystals,[19,20,35] microcrystals and films,[36,37] of $CsPbCl_3$. It should be noted, however, that in nanocrystals this peak is shifted towards higher energy,[38,39] similar to what is observed in other inorganic halide perovskites.[40] This emission peak is commonly attributed to the recombination of bound excitons. There is also consensus in the literature on the interpretation of the emission emerging with cooling at the low-energy side of the luminescence spectra of lead-based perovskites (shoulder 3). It is assigned to the radiative recombination of trapped excitons.[20,23,28,35,40] The low-energy peak 2 has been reported only in a few luminescence studies of $CsPbCl_3$ bulk crystals.[19,35] Similarly, the structured luminescence has been observed in $CsPbBr_3$ and there is extensive discussion regarding its origin. Although the exact nature of the band remains unclear, the most plausible explanations are self-trapped exciton,[41] re-absorption effect,[42] bulk vs surface recombination[43] and Rashba-splitting.[44]

Another interesting feature of the X-ray luminescence of $CsPbCl_3$ crystals is the abnormal shift of the main emission bands with temperature as shown in the insert of Fig. 2. Both emission bands exhibit a blue shift with rising temperature. The intensity of peak 1 decreases and it amalgamates with peak 2 above 50 K. The band formed by merging continues to shift towards the blue with heating until temperature reaches 100 K. Above that, the emission band exhibits a steady spectral shift towards the red with increasing temperature. A similar behaviour of the emission bands has been previously observed in $CsPbBr_3$.[28]

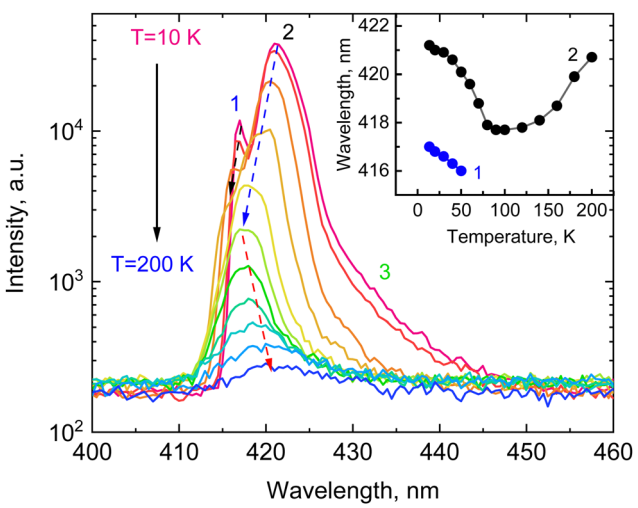

Fig. 2 X-ray luminescence spectra of a $CsPbCl_3$ crystal measured at different temperatures displayed in logarithmic scale. Dashed arrows show the direction of shift for peaks 1 and 2 with temperature. The insert shows the shift of emission peaks 1 and 2 as a function of temperature.

The temperature shift of the edge emission of semiconductors correlates with the temperature evolution of the band gap that is mainly due to electron–phonon interaction. It causes changes in the band structure due to lattice vibrations resulting in a decrease of the band gap with increasing temperature.[45] The thermal expansion of the lattice is considered as a second factor that contributes to these changes. It can cause either a decrease or an increase of the band gap depending on the detailed structure of the valence and conduction bands. Studies of the temperature-dependent luminescence of perovskites reveal that thermal expansion with heating is a main factor that controls the position of the band gap at low temperatures.[46,47] The valence band maximum of lead-halide perovskites is formed by hybridisation of states of Pb and halide ions.[48,49]

To elucidate the origin of the top of the valence band (VB) and the bottom of the (CB) in $CsPbCl_3$, we carried out first-principles calculations using density functional theory. The DOS and PDOS for $CsPbCl_3$ in the low-temperature orthorhombic phase are plotted in Fig. 3. The core Cs ion p-states, which form narrow bands located deep at about −10.9 eV have almost no effect on the VB or CB. The hybridized Pb s-states, and the Cl s-states can be observed deep on the energy scale between −13.8 and −7.8 eV. The top of the VB is mainly formed by Cl p-orbitals with smaller contribution of Pb s- and p-orbitals while the bottom of the conduction band is predominantly formed by hybridized p-states of lead. Cs p-orbitals and Cl p-orbitals contribute to the upper part of the CB. Thermal expansion of the crystal lattice with an increase of temperature may weaken the interaction between these states, leading to a reduction of the width of the valence band and an increase of the forbidden band gap. This causes a blue shift of the edge emission, which is consistent with the high-energy shift of the exciton band observed in the reflection spectra of $CsPbCl_3$ crystals.[50] However, as the temperature rises the electron–phonon interaction starts to dominate, leading to a decrease of the band gap and a red shift of the emission band. Such behaviour of the band gap can explain the observed temperature shift of the $CsPbCl_3$ emission bands.

3.3. Dynamics of X-ray excited emission with temperature

The dynamic of the radiative decay of X-ray emission was investigated over the low-temperature range by using pulsed excitation at a synchrotron source. Fig. 4a illustrates the temperature evolution of decay curves of the $CsPbCl_3$ crystal, measured for excitation by monochromatic X-rays with an energy of 14 keV. The decay curves recorded for the entire emission spectrum of the sample exhibit very fast, non-exponential kinetics. This is due to contributions from different recombination processes and emission centers that is a typical feature of lead-based halide perovskites. The decay kinetics experiences significant changes in shape with decrease of temperature: the peak intensity promptly increases; the long decay component emerges at *ca.* 90 K and its contribution continues to increase at cooling.

To facilitate quantitative analysis of the measured decay curves they were fitted with a sum of exponential functions: $f(t) = \sum_i A_i \exp(-t/\tau_i) + y_o$, where A_i is the amplitude, τ_i the

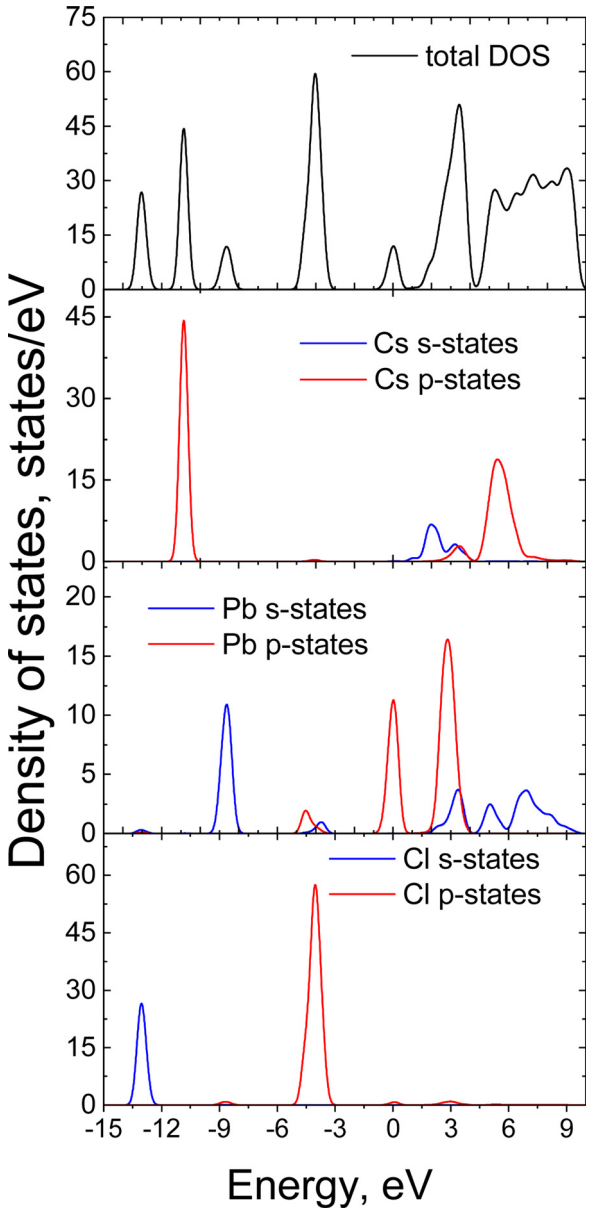

Fig. 3 The DOS and PDOS calculated using the GGA-PBEsol+U functional for orthorhombic $CsPbCl_3$.

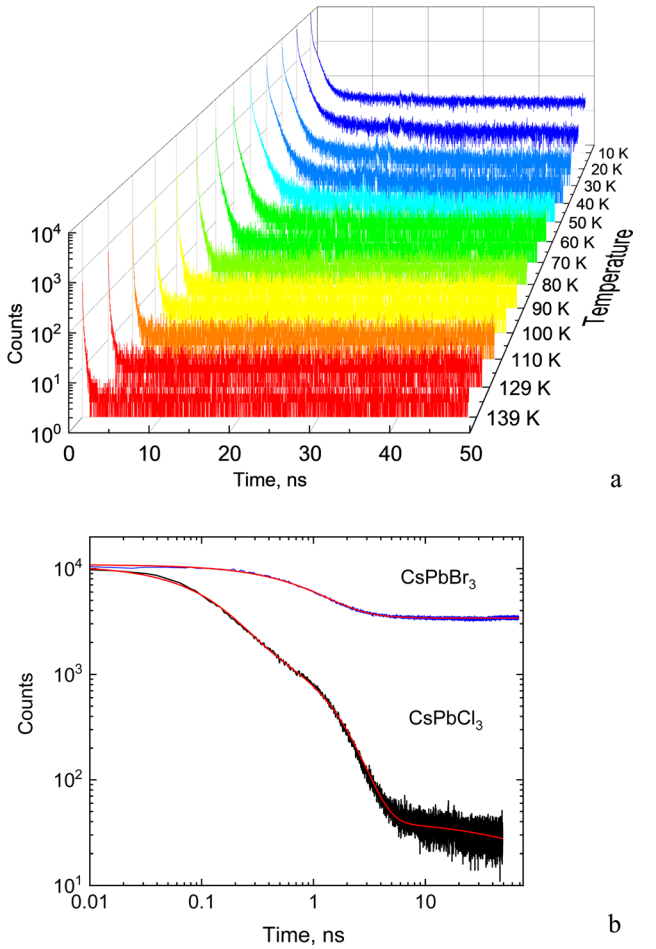

Fig. 4 (a) Decay curves of X-ray luminescence measured in the $CsPbCl_3$ crystal as temperature reduced down to 10 K. The luminescence is excited by X-ray pulses of synchrotron radiation (E = 14 keV). (b) Comparison of decay curves of $CsPbCl_3$ and $CsPbBr_3$ crystals measured at 10 K under the same experimental conditions. The red lines show the fit of experimental data by a sum of exponential functions.

decay time constant and y_0 the background. It should be noted that the multi-exponential fit is widely applied to quantify the processes of recombination decay in semiconductors. Two exponents provided adequate fitting at $T > 90$ K while to account for the occurrence of the slow emission component at lower temperatures we introduced a third component resulting in R-square better than 0.99. The parameters derived from the fit are summarized in Fig. 5a and b. The amplitudes of A_1, A_2 and y_0 exhibit a similar trend; they all decrease as the temperature rises. The third component (A_3) provides a considerable contribution to the decay kinetics of $CsPbCl_3$ at 40 K, while its amplitude rapidly reduces at lower and higher temperatures. Notably, this correlates with the temperature changes of the slow decay component amplitude observed recently in the study of luminescence kinetics of $CsPbBr_3$.[28]

Analysis of these results demonstrates that $CsPbCl_3$ exhibits much faster decay kinetics in comparison with other cesium lead halides.[39,51] This is clearly seen from the juxtaposition of the decay curves of the two crystals displayed in Fig. 4b. The measured fast decay constant τ_1 is *ca.* 0.1 ns which is one order of magnitude less than what has been found in the X-ray luminescence kinetics of $CsPbBr_3$.[28] This value is also consistent with the decay time constant reported in recent studies of the luminescence kinetics of $CsPbCl_3$ microcrystals.[37] Two other decay constants τ_2 and τ_3 derived from the fitting are about one and two order of magnitude larger. As can be seen from Fig. 5a, all decay time constants decrease with rising temperature. It should be noted that this behavior is different from what is typically reported for nanocrystals where the short decay component increases with rising temperature while the slow one decreases.[39,41,52,53]

In line with previous studies, we attribute the fast (τ_1) and middle (τ_2) components in the emission of $CsPbCl_3$ to the radiative decay of bound excitons. The delayed component τ_2

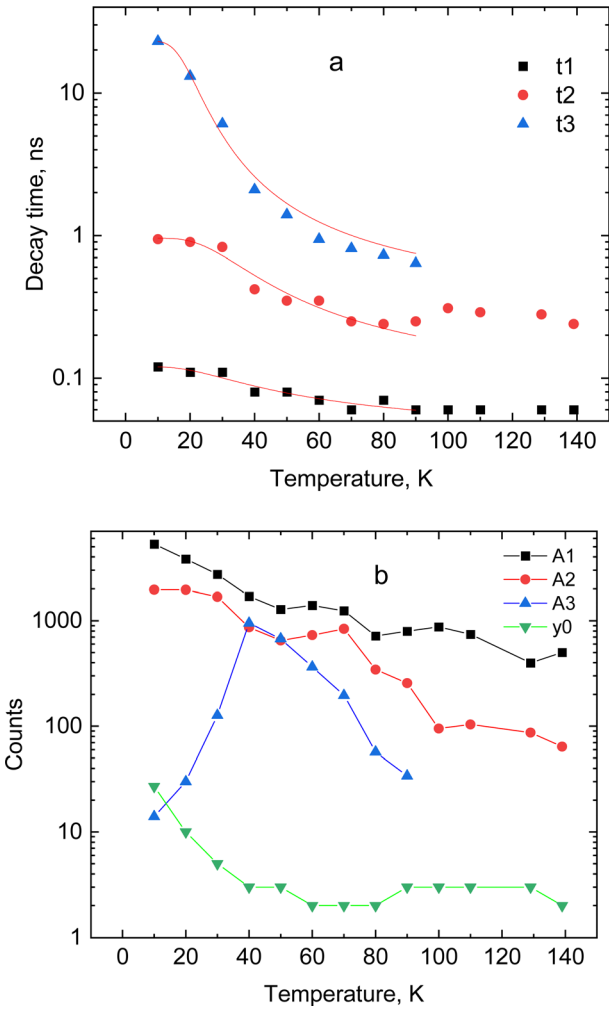

Fig. 5 Temperature dependence of decay constants (a) and amplitudes with background (b) obtained from the fitting of decay curves for $CsPbCl_3$ using a sum of exponential functions: the lines in (a) show the best fit to the temperature dependence of the decay constant $\tau_i = f(T)$ using the model of thermally activated transitions (eqn (1)).

with decay time ~1 ns appears because of formation of bound excitons released from shallow trap states.[28,40] The slow emission component (τ_3), observed below 80 K, is assigned to the radiative recombination of the trapped excitons. This is a thermally activated process and, subsequently, the emission is very slow at low temperature: it mostly contributes to the background at very low temperatures but with increasing temperature this component starts to emerge in the decay curve. The amplitude of this component gradually increases until the onset of the non-radiative quenching. This behaviour of the slow decay is consistent with the changes in the amplitude of this component with temperature, mentioned above.

The observed temperature dependences of the decay rates are very typical for an emission that is governed by processes of thermally activated depopulation of excited states. As the temperature increases the bound and trapped excitons can be released, captured by traps, and subsequently decay non-radiatively. The process of such thermally driven changes can be quantified through a simple model that expresses the relationship between the decay rate and temperature as:

$$\frac{1}{\tau_i} = \frac{1}{\tau_{0i}} + K_i \exp\left(-\frac{\Delta E_i}{kT}\right), \quad (1)$$

where τ_{0i} is the luminescence decay time constant at $T = 0$ K, K_i is the deactivation rate, ΔE_i is the thermal activation energy for the process in question, k is Boltzmann's constant and i =1, 2 and 3. The fit of the data displayed in Fig. 5a yields values of $K_i \sim 10^9$–10^{10} s^{-1} and ΔE in the 6–10 meV range, suggesting efficient delocalization and de-trapping of excitons even at low temperatures. As the temperature increases the excitons can delocalize or escape the traps and start migrating across the crystal until they reach a quenching centre and decay non-radiatively.

3.4. Low temperature scintillation properties

The results for $CsPbCl_3$ demonstrated that at low temperatures the crystal exhibits a bright and very prompt luminescence response under X-ray excitation thus satisfying two key attributes of a scintillator. To assess the potential of this material for the detection of ionizing radiation we measured the light output for excitation with alpha particles. The pulse height spectrum of $CsPbCl_3$ shown in Fig. 6a features a well-resolved peak, caused by 5.49 MeV α-particles from an ^{241}Am source depositing their kinetic energy in the crystal. The peak position is proportional to the light output of the crystal, allowing a study of the variation of scintillation light yield with temperature.[31] Fig. 6b shows that the scintillation efficiency of $CsPbCl_3$ remains roughly constant for temperatures below ca 50 K and above that it decreases with heating. Such behaviour of the light yield as a function of temperature is a common feature observed for the majority of undoped scintillators, and is explained by the thermal quenching effect.[54] The temperature dependence of scintillation light output can be fitted by the classic Mott formula:

$$I = I_0 / \left(1 + K \exp\left(-\frac{E}{kT}\right)\right), \quad (2)$$

where I_0 is the initial luminescence intensity, K is a constant, E is the thermal activation energy of the thermal quenching process, k is Boltzmann's constant. Fitting the $I = f(T)$ plot with eqn (2) gave a value of 34 ± 1 meV for the characteristic activation energy of non-radiative thermal quenching in $CsPbCl_3$.

Theoretical estimates of the scintillation efficiency of $CsPbCl_3$ carried out using a semi-empirical approach[54] gave an upper limit for the absolute light yield of 81300 ph per MeV. The light yield was calculated using the following equation:

$$\mathrm{LY} = \frac{10^6}{2.35E_g}\left[1 + 0.158 \times 10^4 \left\{\frac{1}{\varepsilon_\infty} - \frac{1}{\varepsilon_{\mathrm{stat}}}\right\}\frac{(h\nu_{\mathrm{LO}})^{\frac{3}{2}}}{1.5E_g}\right]^{-1} (\mathrm{ph\,per\,MeV}) \quad (3)$$

Here E_g = 3.05 eV is the band gap energy of $CsPbCl_3$,[39] $\varepsilon_{\mathrm{stat}}$ = 15.7 and ε_∞ = 3.7[55] are the static and high-frequency relative permittivity, $h\nu_{\mathrm{LO}}$ = 46 meV[56] is the maximum energy of LO

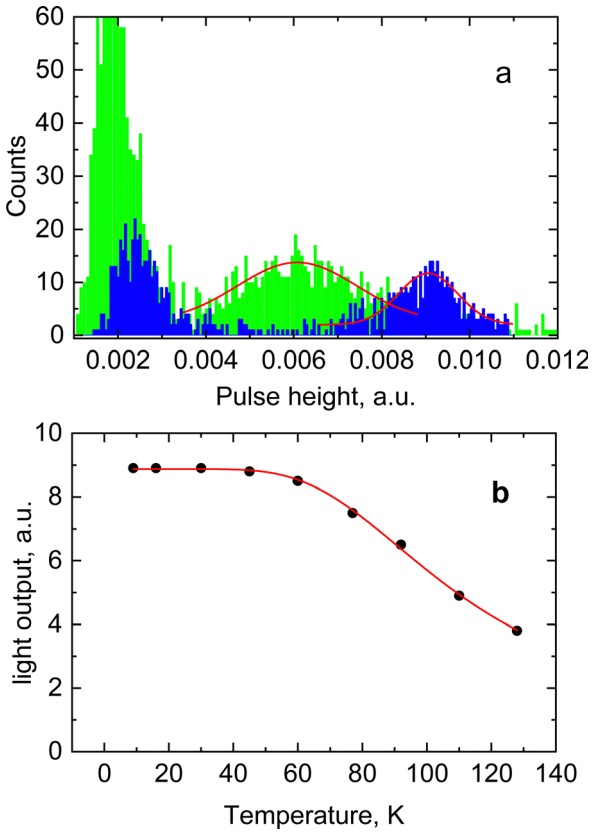

Fig. 6 (a) Pulse height spectra of scintillations caused by α-particles (5.5 MeV) from a ^{241}Am source with $CsPbCl_3$ at 7 K (blue) and LYSO-Ce (green) at 295 K. The red line shows the fitting of a Gaussian to the peak that is attributed to α-particle interaction. The rise of the signal near the origin is due to the detector threshold. (b) The light output of $CsPbCl_3$ as function of temperature for α-particle excitation. The red line shows the best fit of the temperature dependence using the model of thermally activated transitions.

phonons. The scintillation light yield was determined experimentally by comparing the pulse height spectrum of $CsPbCl_3$ displayed in Fig. 5a with data from a reference LYSO-Ce scintillator. The light yield was obtained assuming that the light collection efficiency is the same for both crystals. Under such assumption the light yield of an unknown crystal can be derived by comparing with a reference scintillator after correction for different spectral sensitivity of the photodetector.[57] From these measurements we estimated that at excitation with α-particles the relative light output of $CsPbCl_3$ at 7 K is equal to 140 ± 15% of LYSO-Ce.

Another estimate of the scintillation light yield can be done by integrating area under the scintillation decay curve detected at pulsed X-ray excitation following the approach that has been suggested by[59] and later tested in ref. 28. The recorded sequences of scintillation pulses from $CsPbCl_3$ and LYSO-Ce excited by X-rays from synchrotron was integrated over time interval of 20 ns. After correction for the spectral response of the detector and taking into account the absolute light yield of LYSO-Ce equal to 34 000 ph per MeV[58] and non-proportionality of the scintillator (55% at 14 keV[60]) the light yield of $CsPbCl_3$ under 14 keV X-ray excitation was found to be 19 000 ± 2000 ph per MeV at 10 K.

The obtained values are more than factor two less than the light yield measured by us in bromide perovskites.[8,28] Note, however, that in $CsPbBr_3$ the very slow component seen as a constant background in the decay curves has much higher amplitude and hence a significant contribution to scintillation. Such a feature is very clearly visible in Fig. 3b. Furthermore, in $CsPbCl_3$ the intensity of the long-wavelength band attributed to the slow recombination luminescence is notably reduced in comparison with $CsPbBr_3$. The reduced contribution from the slow recombination emission is likely to cause a decrease of the total scintillation light yield of the $CsPbCl_3$ crystal. Crucially, a decrease of the slow component is always beneficial from the viewpoint of practical applications of scintillators as this allows a reduction of pile-up and facilitates fast counting. Overall, an estimate of the initial photon density calculated as a ratio of light yield to effective decay time constant shows that in $CsPbCl_3$ this parameter is compatible with those observed in other perovskites at low temperatures.

4. Conclusion

In summary, we studied the scintillation and luminescence properties of a $CsPbCl_3$ single crystal as function of temperature using X-rays and particle excitation. It has been found that at low temperature the crystal exhibits an intense narrow-band blue emission due to the radiative decay of bound and trapped excitons. The emission is very sensitive to temperature and quenches at higher temperatures. The scintillation light yield for excitation with α-particles from an ^{241}Am source was estimated to be equal to 140 ± 15% of LYSO-Ce at 7 K. Studies of the luminescence kinetics of $CsPbCl_3$ with pulsed X-ray excitation from a synchrotron showed that the crystal exhibits a very fast decay component at low temperatures. In contrast to bromide perovskites, the decay curves of $CsPbCl_3$ show a small contribution of a very slow decay component which is due to recombination processes. These findings evidence that the crystal is excellent for applications that rely on fast scintillation response at cryogenic temperatures.

Author contributions

V. B. M. instigated the idea of the study, A. V. and Y. C. provided the crystal samples, H. K designed electronic and software for scintillation detection, V. B. M. designed and supervised the experiments and analysed the results, N. V. assisted in setting up the experiment at synchrotron, V. B. M., V. K. and M. R. conducted the measurements, L. V. measured and analysed XRD data, V. K. carried out theoretical modelling, V. B. M. drafted the manuscript, H. K. and V. B. M. edited the manuscript. All authors contributed to the manuscript revision.

Conflicts of interest

There are no conflicts of interest to declare.

Acknowledgements

The work was partially supported by the Ministry of Education and Science of Ukraine. Measurements at B16 beamline of Diamond Light Source were supported through the proposal NT31228.

References

1 S. Yakunin, D. N. Dirin, Y. Shynkarenko, V. Morad, I. Cherniukh, O. Nazarenko, D. Kreil, T. Nauser and M. V. Kovalenko, Detection of gamma photons using solution-grown single crystals of hybrid lead halide perovskites, *Nat. Photonics*, 2016, **10**, 585–589.

2 H. T. Wei and J. S. Huang, Halide lead perovskites for ionizing radiation detection, *Nat. Commun.*, 2019, **10**, 1066.

3 M. Sytnyk, S. Deumel, S. F. Tedde, G. J. Matt and W. Heiss, A perspective on the bright future of metal halide perovskites for X-ray detection, *Appl. Phys. Lett.*, 2019, **115**, 190501.

4 Q. Chen, J. Wu, X. Ou, B. Huang, J. Almutlaq, A. A. Zhumekenov, X. Guan, S. Han, L. Liang, Z. Yi, J. Li, X. Xie, Y. Wang, Y. Li, D. Fan, D. B. L. Teh, A. H. All, O. F. Mohammed, O. M. Bakr, T. Wu, M. Bettinelli, H. Yang, W. Huang and X. Liu, All-inorganic perovskite nanocrystal scintillators, *Nature*, 2018, **561**, 88–93.

5 Y. Zhang, R. Sun, X. Ou, K. Fu, Q. Chen, Y. Ding, L. J. Xu, L. Liu, Y. Han, A. V. Malko, X. Liu, H. Yang, O. M. Bakr, H. Liu and O. F. Mohammed, Metal Halide Perovskite Nanosheet for X-ray High-Resolution Scintillation Imaging Screens, *ACS Nano*, 2019, **13**, 2520–2525.

6 M. Gandini, I. Villa, M. Beretta, C. Gotti, M. Imran, F. Carulli, E. Fantuzzi, M. Sassi, M. Zaffalon, C. Brofferio, L. Manna, L. Beverina, A. Vedda, M. Fasoli, L. Gironi and S. Brovelli, Efficient, fast and reabsorption-free perovskite nanocrystal-based sensitized plastic scintillators, *Nat. Nanotechnol.*, 2020, **15**, 462–468.

7 F. Cao, D. J. Yu, W. B. Ma, X. B. Xu, B. Cai, Y. M. Yang, S. N. Liu, L. H. He, Y. B. Ke, S. Lan, K. L. Choy and H. B. Zeng, Shining Emitter in a Stable Host: Design of Halide Perovskite Scintillators for X-ray Imaging from Commercial Concept, *ACS Nano*, 2020, **14**, 5183–5193.

8 V. B. Mykhaylyk, H. Kraus and M. Saliba, Bright and fast scintillation of organolead perovskite $MAPbBr_3$ at low temperatures, *Mater. Horiz.*, 2019, **6**, 1740–1747.

9 F. Maddalena, L. Tjahjana, A. Z. Xie, G. Arramel, S. W. Zeng, H. Wang, P. Coquet, W. Drozdowski, C. Dujardin, C. Dang and M. D. Birowosuto, Inorganic, Organic, and Perovskite Halides with Nanotechnology for High-Light Yield X- and gamma-ray Scintillators, *Crystals*, 2019, **9**, 88.

10 F. G. Zhou, Z. Z. Li, W. Lan, Q. Wang, L. M. Ding and Z. W. Jin, Halide Perovskite, a Potential Scintillator for X-Ray Detection, Small, *Methods*, 2020, **4**, 2000506.

11 Y. Zhou, J. Chen, O. M. Bakr and O. F. Mohammed, Metal Halide Perovskites for X-ray Imaging Scintillators and Detectors, *ACS Energy Lett.*, 2021, **6**, 739–768.

12 L. Protesescu, S. Yakunin, M. I. Bodnarchuk, F. Krieg, R. Caputo, C. H. Hendon, R. X. Yang, A. Walsh and M. V. Kovalenko, Nanocrystals of Cesium Lead Halide Perovskites (CsPbX(3), X = Cl, Br, and I): Novel Optoelectronic Materials Showing Bright Emission with Wide Color Gamut, *Nano Lett.*, 2015, **15**, 3692–3696.

13 J. H. Heo, D. H. Shin, J. K. Park, D. H. Kim, S. J. Lee and S. H. Im, High-Performance Next-Generation Perovskite Nanocrystal Scintillator for Nondestructive X-Ray Imaging, *Adv. Mater.*, 2018, **30**, 1801743.

14 H. Chen, Q. Wang, G. Peng, S. Wang, Y. Lei, H. Wang, Z. Yang, J. Sun, N. Li, L. Zhao, W. Lan and Z. Jin, Cesium Lead Halide Nanocrystals based Flexible X-Ray Imaging Screen and Visible Dose Rate Indication on Paper Substrate, *Adv. Opt. Mater.*, 2022, **10**, 2102790.

15 T. M. Demkiv, S. V. Myagkota, T. Malyi, A. S. Pushak, V. V. Vistovskyy, P. M. Yakibchuk, O. V. Shapoval, N. E. Mitina, A. S. Zaichenko and A. S. Voloshinovskii, Luminescence properties of CsPbBr3 nanocrystals dispersed in a polymer matrix, *J. Lumin.*, 2018, **198**, 103–107.

16 A. Magi, M. Koshimizu, A. Sato, Y. Fujimoto, S. Kishimoto, T. Yanagida and K. Asai, Development of plastic scintillators loaded with perovskite quantum dots, *Jpn. J. Appl. Phys.*, 2022, **61**, SB1036.

17 A. Voloshinovskii, S. Myagkota, I. Garapyn, G. Stryganyuk, P. Rodnyi and C. W. E. van Eijk, Optical properties of Pb-based aggregated phases in CsBr crystal, *J. Lumin.*, 2005, **111**, 47–51.

18 R. T. Williams, W. W. Wolszczak, X. H. Yan and D. L. Carroll, Perovskite Quantum-Dot-in-Host for Detection of Ionizing Radiation, *ACS Nano*, 2020, **14**, 5161–5169.

19 A. S. Voloshinovskii, V. B. Mikhailik, S. V. Myagkota, M. S. Pidzyrailo and I. P. Pashuk, I. P Exciton luminescence of ionic semiconductors CsPbX3 (X = Cl, Br, I), Ukrainian, *J. Phys.*, 1993, **38**, 112–115.

20 M. Sebastian, J. A. Peters, C. C. Stoumpos, J. Im, S. S. Kostina, Z. Liu, M. G. Kanatzidis, A. J. Freeman and B. W. Wessels, Excitonic emissions and above-band-gap luminescence in the single-crystal perovskite semiconductors CsPbBr3 and $CsPbCl_3$, *Phys. Rev. B: Condens. Matter Mater. Phys.*, 2015, **92**, 235210.

21 M. Kobayashi, K. Omata, S. Sugimoto, Y. Tamagawa, T. Kuroiwa, H. Asada, H. Takeuchi and S. Kondo, Scintillation characteristics of $CsPbCl_3$ single crystals, *Nucl. Instrum. Methods Phys. Res., Sect. A*, 2008, **592**, 369–373.

22 M. D. Birowosuto, F. Maddalena, A. Xie, M. Witkowski, M. Makowski, W. Drozdowski, P. Coquet, C. Dujardin and C. Dang, Scintillators, from solution processable perovskite halide single crystals or quantum dots: the good, the bad, and the ugly, *Proc. SPIE*, 2020, **11494**, 1149415.

23 M. D. Birowosuto, D. Cortecchia, W. Drozdowski, K. Brylew, W. Lachmanski, A. Bruno and C. Soci, X-ray Scintillation in Lead Halide Perovskite Crystals, *Sci. Rep.*, 2016, **6**, 37254.

24 V. B. Mikhailik and H. Kraus, Cryogenic scintillators in searches for extremely rare events, *J. Phys. D: Appl. Phys.*, 2006, **39**, 1181–1191.

25 D. Poda, Scintillation in Low-Temperature Particle Detectors, *Physics*, 2021, **3**, 473–535.

26 S. E. Derenzo, E. Bourret-Courshesne, G. Bizarri and A. Canning, Bright and ultra-fast scintillation from a semiconductor?, *Nucl. Instrum. Methods Phys. Res., Sect. A*, 2016, **805**, 36–40.

27 V. B. Mykhaylyk, H. Kraus, L. Bobb, R. Gamernyk and K. Koronski, Megahertz non-contact luminescence decay time cryothermometry by means of ultrafast PbI2 scintillator, *Sci. Rep.*, 2019, **9**, 5274.

28 V. B. Mykhaylyk, H. Kraus, V. Kapustianyk, H. J. Kim, P. Mercere, M. Rudko, P. Da Silva, O. Antonyak and M. Dendebera, Bright and fast scintillations of an inorganic halide perovskite CsPbBr3 crystal at cryogenic temperatures, *Sci. Rep.*, 2020, **10**, 8601.

29 L. Akselrud and Y. Grin, WinCSD: software package for crystallographic calculations (Version 4), *J. Appl. Crystallogr.*, 2014, **47**, 803–805.

30 I. P. Pashuk, Peculiarities of exciton-phonon interaction in $CsPbCl_3$, *Phys. Electron.*, 1980, **21**, 49–51.

31 V. B. Mikhailik and H. Kraus, Development of techniques for characterisation of scintillation materials for cryogenic application, *Radiat. Meas.*, 2013, **49**, 7–12.

32 P. Giannozzi, O. Andreussi, T. Brumme, O. Bunau, M. Buongiorno Nardelli, M. Calandra, R. Car, C. Cavazzoni, D. Ceresoli, M. Cococcioni, N. Colonna, I. Carnimeo, A. Dal Corso, S. de Gironcoli, P. Delugas, R. A. DiStasio, Jr., A. Ferretti, A. Floris, G. Fratesi, G. Fugallo, R. Gebauer, U. Gerstmann, F. Giustino, T. Gorni, J. Jia, M. Kawamura, H. Y. Ko, A. Kokalj, E. Küçükbenli, M. Lazzeri, M. Marsili, N. Marzari, F. Mauri, N. L. Nguyen, H. V. Nguyen, A. Otero-de-la-Roza, L. Paulatto, S. Poncé, D. Rocca, R. Sabatini, B. Santra, M. Schlipf, A. P. Seitsonen, A. Smogunov, I. Timrov, T. Thonhauser, P. Umari, N. Vast, X. Wu and S. Baroni, Advanced capabilities for materials modelling with Quantum ESPRESSO, *J. Phys.: Condens. Matter*, 2017, **29**, 465901.

33 M. R. Linaburg, E. T. McClure, J. D. Majher and P. M. Woodward, $Cs_{1-x}Rb_xPbCl_3$ and $Cs_{1-x}Rb_xPbBr_3$ Solid Solutions: Understanding Octahedral Tilting in Lead Halide Perovskites, *Chem. Mater.*, 2017, **29**, 3507–3514.

34 Y. H. He, C. C. Stoumpos, I. Hadar, Z. Z. Luo, K. M. McCall, Z. F. Liu, D. Y. Chung, B. W. Wessels and M. G. Kanatzidis, Demonstration of Energy-Resolved gamma-Ray Detection at Room Temperature by the $CsPbCl_3$ Perovskite Semiconductor, *J. Am. Chem. Soc.*, 2021, **143**, 2068–2077.

35 K. Watanabe, M. Koshimizu, T. Yanagida, Y. Fujimoto and K. Asai, Luminescence and scintillation properties of La- and La,Ag-doped $CsPbCl_3$ single crystals, *Jpn. J. Appl. Phys.*, 2016, **55**, 02BC20.

36 S. Kondo, H. Ohsawa, T. Saito, H. Asada and H. Nakagawa, Room-temperature stimulated emission from microcrystalline $CsPbCl_3$ films, *Appl. Phys. Lett.*, 2005, **87**, 131912.

37 N. Falsini, N. Calisi, G. Roini, A. Ristori, F. Biccari, P. Scardi, C. Barri, M. Bollani, S. Caporali and A. Vinattieri, Large-Area Nanocrystalline Caesium Lead Chloride Thin Films: A Focus on the Exciton Recombination Dynamics, *Nanomaterials*, 2021, **11**, 434.

38 J. Yi, X. Ge, E. Liu, T. Cai, C. Zhao, S. Wen, H. Sanabria, O. Chen, A. M. Rao and J. Gao, The correlation between phase transition and photoluminescence properties of $CsPbX_3$ (X = Cl, Br, I) perovskite nanocrystals, *Nanoscale Adv.*, 2020, **2**, 4390–4394.

39 B. T. Diroll, H. Zhou and R. D. Schaller, Low-Temperature Absorption, Photoluminescence, and Lifetime of CsPbX3 (X = Cl, Br, I) Nanocrystals, *Adv. Funct. Mater.*, 2018, **28**, 1800945.

40 C. Roda, M. Fasoli, M. L. Zaffalon, F. Cova, V. Pinchetti, J. Shamsi, A. L. Abdelhady, M. Imran, F. Meinardi, L. Manna, A. Vedda and S. Brovelli, Understanding Thermal and A-Thermal Trapping Processes in Lead Halide Perovskites Towards Effective Radiation Detection Schemes, *Adv. Funct. Mater.*, 2021, **31**, 2104879.

41 F. Pan, J. Li, X. Ma, Y. Nie, B. Liu and H. Ye, Free and self-trapped exciton emission in perovskite CsPbBr3 microcrystals, *RSC Adv.*, 2022, **12**, 1035–1042.

42 K. Schötz, A. M. Askar, W. Peng, D. Seeberger, T. P. Gujar, M. Thelakkat, A. Köhler, S. Huettner, O. M. Bakr, K. Shankar and F. Panzer, Double peak emission in lead halide perovskites by self-absorption, *J. Mater. Chem. C*, 2020, **8**, 2289–2300.

43 S. T. Birkhold, E. Zimmermann, T. Kollek, D. Wurmbrand, S. Polarz and L. Schmidt-Mende, Impact of Crystal Surface on Photoexcited States in Organic-Inorganic Perovskites, *Adv. Funct. Mater.*, 2017, **27**, 1604995.

44 B. Wu, H. Yuan, Q. Xu, J. A. Steele, D. Giovanni, P. Puech, J. Fu, Y. F. Ng, N. F. Jamaludin, A. Solanki, S. Mhaisalkar, N. Mathews, M. B. J. Roeffaers, M. Gratzel, J. Hofkens and T. C. Sum, Indirect tail states formation by thermal-induced polar fluctuations in halide perovskites, *Nat. Commun.*, 2019, **10**, 484.

45 M. Cardona, T. A. Meyer and M. L. W. Thewalt, Temperature dependence of the energy gap of semiconductors in the low-temperature limit, *Phys. Rev. Lett.*, 2004, **92**, 196403.

46 K. Wei, Z. Xu, R. Chen, X. Zheng, X. Cheng and T. Jiang, Temperature-dependent excitonic photoluminescence excited by two-photon absorption in perovskite CsPbBr3 quantum dots, *Opt. Lett.*, 2016, **41**, 3821–3824.

47 S. Wang, J. Ma, W. Li, J. Wang, H. Wang, H. Shen, J. Li, J. Wang, H. Luo and D. Li, Temperature-Dependent Band Gap in Two-Dimensional Perovskites: Thermal Expansion Interaction and Electron–Phonon Interaction, *J. Phys. Chem. Lett.*, 2019, **10**, 2546–2553.

48 M. Ahmad, G. Rehman, L. Ali, M. Shafiq, R. Iqbal, R. Ahmad, T. Khan, S. Jalali-Asadabadi, M. Maqbool and I. Ahmad, Structural, electronic and optical properties of CsPbX3 (X = Cl, Br, I) for energy storage and hybrid solar cell applications, *J. Alloys Compd.*, 2017, **705**, 828–839.

49 M. Kovalenko, O. Bovgyra and V. Kolomiets, Structure and electronic properties of CsPbBr3 perovskite, *J. Phys. Stud.*, 2021, **25**, 4701.

50 O. N. Yunakova, V. K. Miloslavsky, E. N. Kovalenko and V. V. Kovalenko, Effect of structural phase transitions on the exciton absorption spectrum of thin $CsPbCl_3$ films, *Low Temp. Phys.*, 2014, **40**, 690–693.

51 L. Chen, B. Li, C. Zhang, X. Huang, X. Wang and M. Xiao, Composition-Dependent Energy Splitting between Bright and Dark Excitons in Lead Halide Perovskite Nanocrystals, *Nano Lett.*, 2018, **18**, 2074–2080.

52 M. Dendebera, Y. Chornodolskyy, R. Gamernyk, O. Antonyak, I. Pashuk, S. Myagkota, I. Gnilitskyi, V. Pankratov, V. Vistovskyy, V. Mykhaylyk, M. Grinberg and A. Voloshinovskii, Time resolved luminescence spectroscopy of CsPbBr3 single crystal, *J. Lumin.*, 2020, **225**, 117346.

53 X. Ma, F. Pan, H. Li, P. Shen, C. Ma, L. Zhang, H. Niu, Y. Zhu, S. Xu and H. Ye, Mechanism of Single-Photon Upconversion Photoluminescence in All-Inorganic Perovskite Nanocrystals: The Role of Self-Trapped Excitons, *J. Phys. Chem. Lett.*, 2019, **10**, 5989–5996.

54 V. B. Mikhailik and H. Kraus, Performance of scintillation materials at cryogenic temperatures, *Phys. Status Solidi B*, 2010, **247**, 1583–1599.

55 M. R. Filip, J. B. Haber and J. B. Neaton, Phonon Screening of Excitons in Semiconductors: Halide Perovskites and Beyond, *Phys. Rev. Lett.*, 2021, **127**, 067401.

56 D. M. Calistru, L. Mihut, S. Lefrant and I. Baltog, Identification of the symmetry of phonon modes in $CsPbCl_3$ in phase IV by Raman and resonance-Raman scattering, *J. Appl. Phys.*, 1997, **82**, 5391–5395.

57 V. Alenkov, O. A. Buzanov, N. Khanbekov, V. N. Kornoukhov, H. Kraus, V. B. Mikhailik and V. A. Shuvaeva, Application of the Monte-Carlo refractive index matching (MCRIM) technique to the determination of the absolute light yield of a calcium molybdate scintillator, *J. Instrum.*, 2013, **8**, P06002–P06002.

58 S. Blahuta, A. Bessière, B. Viana, P. Dorenbos and V. Ouspenski, Evidence and Consequences of Ce 4+ in LYSO:Ce,Ca and LYSO:Ce,Mg Single Crystals for Medical Imaging Applications, *IEEE Trans. Nucl. Sci.*, 2013, **60**, 3134–3141.

59 S. E. Derenzo, M. J. Weber and M. K. Klintenberg, Temperature dependence of the fast, near-band-edge scintillation from CuI, HgI_2, PbI_2, ZnO: Ga and CdS: In, *Nucl. Instrum. Methods Phys. Res., Sect. A*, 2002, **486**, 214–219.

60 I. V. Khodyuk, J. T. M. de Haas and P. Dorenbos, Nonproportional Response Between 0.1–100 keV Energy by Means of Highly Monochromatic Synchrotron X-Rays, *IEEE Trans. Nucl. Sci.*, 2010, **57**, 1175–1181.